Glacial-Interglacial Variations in Organic Carbon Burial in the Northwest Pacific Ocean Over the Last 380 kyr and its Environmental Implications

Yuying Zhang[1], Limin Hu[1,2,3]*, Yonghua Wu[2,3], Zhi Dong[3], Zhengquan Yao[2,3], Xun Gong[4,5], Yanguang Liu[2,3], Minoru Ikehara[6] and Xuefa Shi[2,3]*

[1]College of Marine Geosciences, Key Laboratory of Submarine Geosciences and Prospecting Technology, Ocean University of China, Qingdao, China, [2]Laboratory for Marine Geology, Pilot National Laboratory for Marine Science and Technology, Qingdao, China, [3]Key Laboratory of Marine Geology and Metallogeny, First Institute of Oceanography, Ministry of Natural Resources, Qingdao, China, [4]Hubei Key Laboratory of Marine Geological Resources, China University of Geosciences, Wuhan, China, [5]Shandong Provincial Key Laboratory of Computer Networks, Qilu University of Technology (Shandong Academy of Sciences), Jinan, China, [6]Center for Advanced Marine Core Research, Kochi University, Kochi, Japan

The carbon cycle on the Earth's surface is linked to long-term variations in atmospheric CO_2 as well as carbon sequestration in various pools. The burial of particulate organic carbon (OC) in marine sediments is also highly sensitive to the global climate over geological time scales, but with little known about OC burial and its regulations over glacial-interglacial cycles. Here, we present a long-term OC record over the past ~380 kyr, from the Northwest Pacific Ocean, an ideal region for studying OC burial and its environmental implications on glacial-interglacial timescales. We observed a distinct cyclicity of higher OC burial in glacial periods, which was coupled with input from Asian dust and the Kuroshio Current but seemingly decoupled from biogenic element contents, implying a limited effect of marine productivity on OC burial. Moreover, the sedimentary record of OC was synchronous with oceanic redox conditions, especially the redox sensitive elements at the sediment-water interface, indicating a relatively reducing conditions that enhanced OC preservation during glacial periods. The overall glacial-interglacial OC burial regime in the Northwest Pacific Ocean was conceptually constructed. It showed a higher efficiency of OC burial during glacial periods and significant degradation during interglacial periods. The findings of this study highlighted the important contribution of environmental redox conditions on OC burial in the deep Northwest Pacific, demonstrating the sensitivity of the carbon cycle to global climate on an orbital scale.

Keywords: organic carbon burial, marine productivity, redox conditions, glacial-interglacial, Northwest Pacific Ocean

1 INTRODUCTION

Oceanic processes account for the observed 80–100 ppm drawdown of atmospheric CO_2 concentration during glacial periods (Kohfeld et al., 2005) with marine sediment as an important reservoir of global organic carbon (OC), constraining air-sea CO_2 flux (Petit et al., 1999; Sigman and Boyle., 2000). Previous studies have suggested that the long-term storage of OC burial in sediments (Hall and McCave, 1998; Agnihotri et al., 2003), which accounts for only a little of the export from the surface, has a very sensitive response to paleoclimate variations (Cartapanis et al., 2016). Moreover, the fate of OC in marine sediments has important implications for oceanic biological, geochemical, and physical processes on glacial-interglacial timescales (LaRowe et al., 2020). For example, the enhanced burial of sedimentary OC during glacial periods is related to increased biological productivity (Sarnthein et al., 1988), higher transfer efficiency from the

exposed continental shelf to the water column (Keil et al., 1997), and/or better preservation under reduced oxygenation (Hoogakker et al., 2015).

Marine primary productivity, which is influenced by iron availability to plankton, ocean nutrient content and utilization, and other factors, removes CO_2 from the air and produces organic matter through photosynthesis and results in OC storage (Kohfeld et al., 2005). Hence, productivity is considered as one of the most important drivers of OC supply and burial (Agnihotri et al., 2003). During OC export to the deeper ocean, there is a continuous loss of vertical transport from the surface (Schoepfer et al., 2015). The continental dust input revealed by deep-sea sediment records generally exhibits fluxes several times higher during glacials compared to interglacials (Anderson et al., 2006; Rea, 2007). This may affect marine productivity (Thöle et al., 2019) as well as OC composition and preservation (Cartapanis et al., 2016). As critical components of the global carbon cycle, OC degradation and
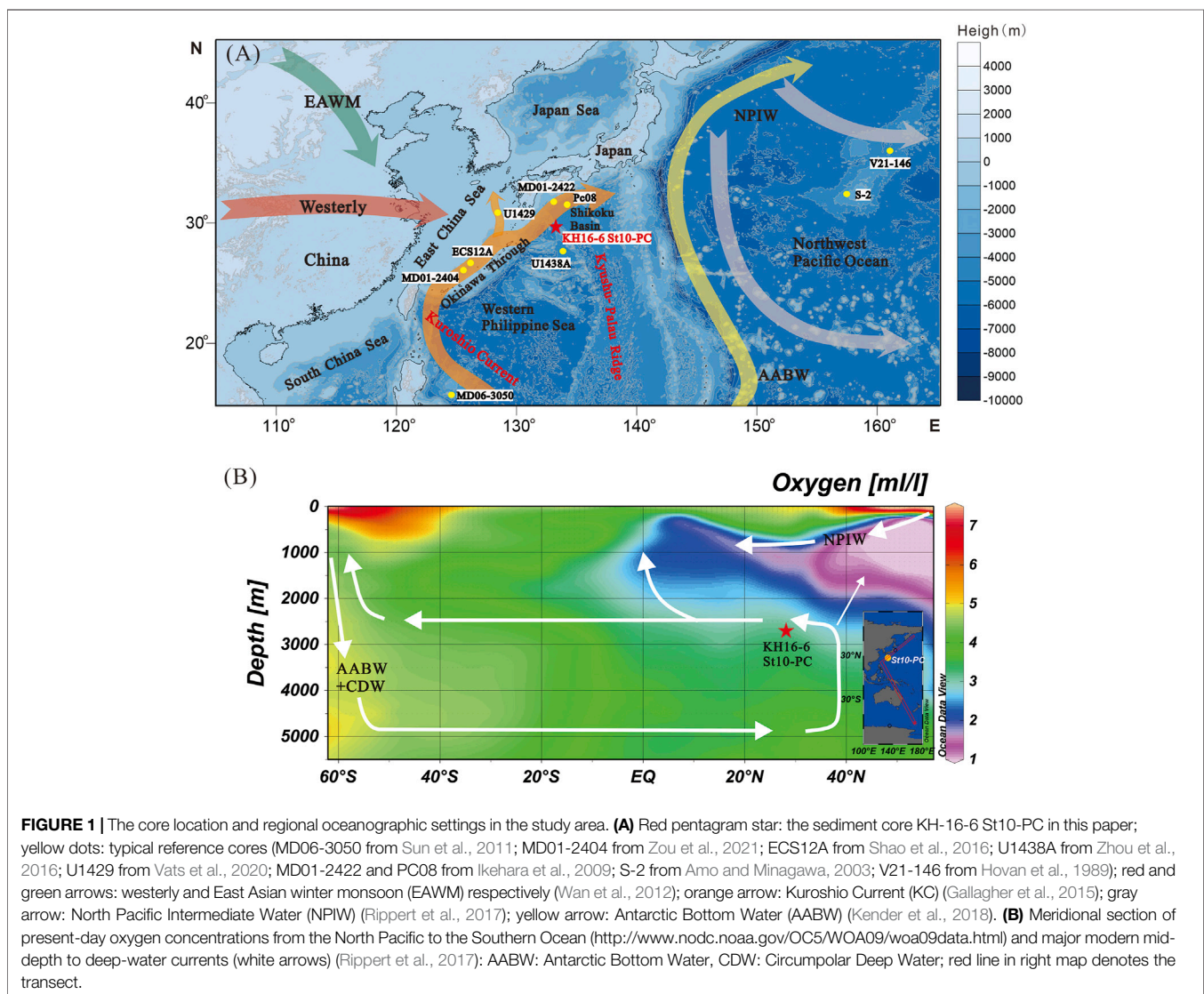

FIGURE 1 | The core location and regional oceanographic settings in the study area. **(A)** Red pentagram star: the sediment core KH-16-6 St10-PC in this paper; yellow dots: typical reference cores (MD06-3050 from Sun et al., 2011; MD01-2404 from Zou et al., 2021; ECS12A from Shao et al., 2016; U1438A from Zhou et al., 2016; U1429 from Vats et al., 2020; MD01-2422 and PC08 from Ikehara et al., 2009; S-2 from Amo and Minagawa, 2003; V21-146 from Hovan et al., 1989); red and green arrows: westerly and East Asian winter monsoon (EAWM) respectively (Wan et al., 2012); orange arrow: Kuroshio Current (KC) (Gallagher et al., 2015); gray arrow: North Pacific Intermediate Water (NPIW) (Rippert et al., 2017); yellow arrow: Antarctic Bottom Water (AABW) (Kender et al., 2018). **(B)** Meridional section of present-day oxygen concentrations from the North Pacific to the Southern Ocean (http://www.nodc.noaa.gov/OC5/WOA09/woa09data.html) and major modern mid-depth to deep-water currents (white arrows) (Rippert et al., 2017): AABW: Antarctic Bottom Water, CDW: Circumpolar Deep Water; red line in right map denotes the transect.

preservation are closely regulated by oceanic redox conditions (LaRowe et al., 2020). It has been shown that most of the OC generated by marine surface production is rapidly oxidized and consumed by microbial degradation (approximately 80–90%) (Opsahl and Benner, 1997), reducing its preservation efficiency to only about 1% (Hedges et al., 1997). The influences of oxygen concentration and exposure time on OC preservation in sediments (Hartnett et al., 1998) are determined by the redox conditions in both the water column and the sediment-water interface, which play significant roles not only in microbial growth and activity (Belanger et al., 2020), but also in microbial oxidation of OC (Anderson et al., 2019).

The Kyushu-Palau Ridge, located in the Northwest Pacific Ocean, is influenced by Asian dust input and complex ocean circulation systems (**Figure 1A**). The special regional setting has important effects on the evolution of the sources and sinks of allochthonous and autochthonous materials and their interaction with global sea-level change (Ikehara et al., 2009; Shao et al., 2016; Li et al., 2017). In this work, the study area is relatively far from the Asian continental shelf (**Figure 1A**). Therefore, the effect of sea-level variation in river input to the study area from the Asian continent is much less than that in marginal seas (Milliman and Farnsworth, 2011). Moreover, adjacent to the Asian dust source area, dust input is one of the primary transport routes for terrestrial organic matter, nutrients, and fine-grain particles to this region (Maher et al., 2010). Various proxies, including grain size end-members (Zhou et al., 2016), geochemical element ratios, and mineral ratios (Seo et al., 2014) have been used to quantify dust fluxes into the Pacific Ocean, showing several times greater dust input during glacial periods than during interglacial periods (Hovan et al., 1989; Wan and Xu, 2017). Furthermore, along the western edge of the North Pacific, the Kuroshio Current (KC) supplies a large quantity of heat and material to the study area and thus plays an important role in controlling the marine environment, ecosystem, and sedimentation (Gallagher et al., 2015). Both modeling and sedimentary proxies were used in previous studies to reconstruct KC intensity on orbital scales in the Northwest Pacific. They indicated the decreased KC during glacials and the strengthened KC during interglacials (Kao et al., 2006; Li et al., 2018; Vats et al., 2020). In addition, the evolution of ocean circulation, comprising several currents occurring at different water depths, including the KC, North Pacific Intermediate Water (NPIW) (Rippert et al., 2017), and southern-sourced deep water as Antarctic Bottom Water (AABW) (Kender et al., 2018) (**Figure 1B**), has a significant effect on oceanic stratification (Jaccard et al., 2005), upwelling (Worne et al., 2019) and redox conditions (Li et al., 2018). Therefore, the intense ocean-land-atmosphere interaction in the Northwest Pacific makes it as an ideal region for studying OC burial and its environmental relationships with paleo-oceanographic conditions over glacial-interglacial cycles. However, long-term records of sedimentary OC burial based on deep-sea sediment cores in the Northwest Pacific have been lack of extensive reconstruction before (Amo and Minagawa, 2003; Ikehara et al., 2009), especially for the comprehensive understanding of the dominant factors that control OC burial over glacial-interglacial cycles.

In the present study, we combined data for sediment grain size, bulk OC content and its stable carbon isotope, biogenic elements, and trace metals in core KH-16-6 St10-PC (hereinafter, St10-PC) from the northern Kyushu-Palau Ridge, which has been well-dated using AMS ^{14}C and δ^{18}O of planktonic foraminifera, in order to determine the long-term record of the glacial-interglacial cyclic OC burial and its constraints over the last 380 kyr. The main objectives were to identify the relationships between long-term OC accumulation and marine productivity evolution as well as the impact of hydrological conditions with redox conditions. Finally, by comparing the orbital-scale OC burial with previously published records, this paper summarized the mechanism of OC burial between glacial and interglacial climate regimes in the Northwest Pacific in a schematic.

2 MATERIALS AND METHODS

2.1 Sampling
The sediment core St10-PC (29°28′N, 133°37′E) (length = 647 cm) was collected at a water depth of 2670 m during the R/V *Hakuho-maru* cruise of KH16-6 in the northern Kyushu-Palau Ridge of the Northwest Pacific (**Figure 1A**). The station is located at approximately 600 km east of Kyushu Island and experiences frequent volcanic eruptions. The sediments of core St10-PC mainly consist of homogeneous brownish-gray silty clay with several volcanic ash layers. A total of 284 samples were delineated at approximately 2 cm intervals for the analyses and stored at −20°C until analysis.

2.2 Analytical Methods
2.2.1 AMS ^{14}C Dating and δ^{18}O Analysis
Accelerator mass spectrometry (AMS) ^{14}C dating was performed by Beta Analytic Laboratory, United States, on the mixed planktonic foraminifera species *Globorotalia inflata* and *Globigernoides ruber*, using the larger than 150 µm size fraction of four samples in the upper core. Calibrated calendar ages were converted using CALIB 7.20, using the MARINE13 database (Reimer et al., 2013) and a local reservoir age of ΔR = 39 ± 18 years (Yoneda et al., 2007). The planktonic foraminifera *G. inflata* (approximately 10 shells, 400–500 µm size fraction) was measured for stable oxygen isotopes (δ^{18}O) using a Finnigan-MAT252 mass spectrometer at Tongji University, Shanghai, China. Precision was validated against a Chinese national carbonate standard (GBW04405) and NBS-19. A total of 280 δ^{18}O data were reported based on the conventional PDB (Pee Dee Belemnite) standard, with a standard deviation of ±0.07‰ (Cheng et al., 2005).

2.2.2 Analysis of Major and Trace Element Concentrations
97 Samples were analyzed for major and trace element concentrations at the Key Laboratory of Marine Geology and Metallogeny, First Institute of Oceanography (FIO), Ministry of Natural Resources (MNR), Qingdao, China. The samples were digested with HNO_3 and HF, and then diluted to 50 ml with Milli-Q water. Finally, major element concentrations were

measured using inductively coupled plasma-optical emission spectrometry (ICP-OES, iCAP 6300, Thermo Fisher Scientific Inc., Waltham, United States), and trace element concentrations were measured using inductively coupled plasma mass spectrometry (ICP-MS, Thermo X Series 2, Thermo Fisher Scientific Inc.). Replicate measurements were conducted on 10% of the samples (randomly selected), and the relative standard deviations were <1% for major elements and <5% for trace elements ($n = 20$) (Zou et al., 2012).

2.2.3 Analysis of Sediment Grain Size, Total Organic Carbon, and $\delta^{13}C_{org}$

The analysis of sediment grain size and total organic carbon (TOC) content were carried out at the Key Laboratory of Marine Geology and Metallogeny, FIO, MNR, Qingdao, China. The detailed analytical methods of sediment grain size and bulk OM proxies can be found in Hu et al. (2012). Grain size samples ($n = 284$) were processed using a laser particle size analyzer (Mastersizer 3000, Malven Instruments Ltd., United Kingdom) after removing organic matter and $CaCO_3$ through H_2O_2 and diluted HCl, respectively. The carbonate-free samples ($n = 278$) for TOC analysis and the bulk sediment samples for total carbon (TC) were analyzed in duplicate in a Vario EL-III Elemental Analyzer (elementar Analysensysteme GmbH, Langenselbold, Germany). Stable carbon isotope composition analysis of OC ($\delta^{13}C_{org}$) was carried out using a Thermo Fisher 253 Plus mass spectrometer (Thermo Fisher Scientific Inc.), at the Pilot National Laboratory for Marine Science and Technology in Qingdao, China. The isotopic values of OC ($n = 278$) are reported in standard δ notation as per mil deviations relative to the PDB carbon standard, with a standard deviation of ±0.1‰.

2.3 Statistical Analysis

The mass accumulation rate (MAR), an index to refer to the sediment fluxes, was calculated by the linear sedimentation rates (LSR) and the dry bulk density (DBD) of the sediment using the following **Eqs 1**, **2**, then the burial fluxes of TOC were determined using **Eq. 3**:

$$\text{LSR (cm/kyr)} = \Delta h / \Delta t \qquad (1)$$

$$\text{MAR (mg/cm}^2\text{/kyr)} = \text{LSR (cm/kyr)} * \text{DBD (g/cm}^3) * 1000 \qquad (2)$$

$$\text{TOC}_{\text{fluxes}} \text{(mg/cm}^2\text{/kyr)} = \text{TOC (\%)} * \text{MAR} \qquad (3)$$

where Δh and Δt are the depth and age differences, respectively, between the two age control points.

The biogenic calcium carbonate ($CaCO_3$) content as determined by inorganic carbon was calculated using **Eq. 4**:

$$\text{CaCO}_3 \text{ (\%)} = (\text{TC} - \text{TOC}) * 8.33 * 100\% \qquad (4)$$

The biogenic barium (Ba_{bio}) content as determined by the major element barium was calculated using **Eq. 5**:

$$\text{w} (Ba_{bio}) = \text{Ba}_{\text{total}} - \text{Al}_{\text{total}} * (\text{Ba/Al})_{\text{terr}} \qquad (5)$$

where w (Ba_{bio}) is the mass fraction of biogenic barium in the sediments (μg/g); Ba_{total}, Al_{total}, and $(Ba/Al)_{terr}$ are the total

barium and aluminum contents in the sediments (μg/g) and terrestrial Ba/Al ratio (0.0041, Shao et al., 2016), respectively.

The end-member statistical analysis employed a MATLAB modeling algorithm (Dietze et al., 2012) to analyze individual grain-size populations (end-member loadings, volume %) and their contributions to bulk grain-size composition (scores, %) (Zhou et al., 2015).

3 RESULTS

3.1 Age Model and Stratigraphic Chronology

In the Northwest Pacific, definite age models of long-term sedimentary cores generally use a comparison between the $\delta^{18}O$ of planktonic foraminifera and the LR04 $\delta^{18}O$ stack of benthic foraminifera in a specific sediment core (Ikehara et al., 2009; Sun et al., 2011; Ujiié et al., 2016). An age model for core St10-PC was reconstructed based on 11 age control points (**Table 1**) provided by the AMS^{14}C dating results and the *G. inflata*-$\delta^{18}O$ records in this core (**Figure 2C**, data are available in the supplementary dataset), and correlating this *G. inflata*-$\delta^{18}O$ records to the standard deep-sea oxygen isotopic LR04-$\delta^{18}O$ stack (**Figure 2E**; Lisiecki and Raymo, 2005) and *G. ruber*-$\delta^{18}O$ records in core MD06-3050 from near Luzon Island in the Philippine Sea (**Figure 2D**, Sun et al., 2011). This age model indicates that core St10-PC covers past ~380 kyr (**Figure 2**), spanning marine isotope stages (MIS) 1–10, which cover nearly five complete glacial-interglacial cycles (**Figure 2**).

According to this chronology, the average LSR was lower than those in other sediment cores from marginal seas (Shao et al., 2016), varying over the range between 0.5 (in Holocene) and 3.6 (in MIS2) cm/kyr, with an average value of 1.8 cm/kyr (**Table 1**; **Figure 2A**). The MAR varied from 353.6 to 3121.8 mg/cm^2/kyr, with average value of 1484.5 mg/cm^2/kyr (**Table 1**; **Figure 2B**). Glacial-interglacial differences in LSR and MAR were evident with higher average values in glacial periods than that in interglacial periods (**Figures 2A,B**), which is thought to primarily reflect the increased terrestrial input (dust input and fluvial discharge) when sea level declined (**Figure 2F**, Waelbroeck et al., 2002).

3.2 Temporal Variations of Total Organic Carbon Fluxes, $\delta^{13}C_{org}$ Values and Biogenic Element Contents

To estimate the TOC-fluxes on orbital scale, we combined the MAR data in this study with the previously reported TOC abundances (Zhang et al., 2020). The TOC-fluxes varied from 0.8 to 11.7 mg/cm^2/kyr (**Figure 3F**), with a mean value of 3.2 mg/cm^2/kyr. Furthermore, the peaks in TOC contents correlated well with their fluxes (**Figures 3F,G**), showing significant cyclic variations that were almost two times higher during glacial periods (particularly in MIS2, $p < 0.01$, **Supplementary Table S1**), which is consistent with hundreds of sedimentary OC burial records around the world (Cartapanis et al., 2016). The TN contents and fluxes (**Supplementary Figures S1B,C**) varied in the similar tendencies

TABLE 1 | Radiocarbon ages with calibrated ages of core St10-PC and control points to construct the age model.

Depth (cm)	AMS^{14}C age (yrs BP)	Calibrated age (yrs BP) (1σ)	MIS periods	Description	LSR (cm/kyr)	MAR (mg/cm^2/kyr)
1.5	3290 ± 30	3075 ± 61	MIS1	AMS^{14}C age	0.5	353.6
32.5	12500 ± 40	13941 ± 74	MIS1/2	AMS^{14}C age	2.9	2410.8
44.5	14480 ± 40	17059 ± 97	MIS2	AMS^{14}C age	3.6	3121.8
62.5	23200 ± 80	27152 ± 128	MIS2/3	AMS^{14}C age	1.8	1592.1
105.0	/	62,000	MIS3/4	δ^{18}O record	1.3	1083.6
130.0	/	76,000	MIS4/5	δ^{18}O record	1.5	1264.7
231.0	/	135,000	MIS5/6	δ^{18}O record	1.8	1416.7
321.0	/	185,000	MIS6/7	δ^{18}O record	1.9	1600.8
413.0	/	248,000	MIS7/8	δ^{18}O record	1.4	1109.7
490.0	/	290,000	MIS8/9	δ^{18}O record	2.0	1559.4
568.0	/	338,000	MIS9/10	δ^{18}O record	1.7	1336.0
647.0	/	380,000	End	δ^{18}O record	1.9	1403.1

The original detailed data supporting this age model are derived from previous works (Zhang et al., 2020) and are shown in supplementary dataset.

as TOC. However, the TOC vs. TN scatter plot (**Supplementary Figure S2**) shows an intercept of 0.026% inorganic nitrogen, which accounts for ~58% of the mean total nitrogen and results in low TOC/TN values downcore, with a range of 2.34–8.47 (**Supplementary Figure S1A**). $\delta^{13}C_{org}$ in core St10-PC varied between -25.24‰ and −21.04‰ (mean: 22.59‰) (**Figure 3E**), trending to more positive during the glacials ($p < 0.01$, **Supplementary Table S1**). The overall more positive $\delta^{13}C_{org}$ values may indicate sedimentary OC mainly derived from marine-sourced contributions (Ikehara et al., 2009; Li et al., 2018).

The abundances of $CaCO_3$ and Ba_{bio} in marine sediments have been widely used as paleo-productivity proxies (Agnihotri et al., 2003; Shao et al., 2016). In this study, $CaCO_3$ and Ba_{bio} contents in core St10-PC ranged from 8.90 to 57.46% and 176.58–512.09 µg/g respectively, with average of 35.56% and 345.68 µg/g (**Figures 3B,D**). Downcore $CaCO_3$ ($p < 0.05$, **Supplementary Table S1**) and Ba_{bio} ($p < 0.01$, **Supplementary Table S1**) were significantly higher during interglacials than glacials, which is consistent with the Ca/Ti and Ba/Al ratios (**Figures 3A,C**), but reversed compared to the OC fluxes (**Figure 3F**).

3.3 Temporal Variations of Redox Sensitive Elements

In this study, the concentrations of trace elements sensitive to the redox conditions of the hydrological regime, such as uranium (U), vanadium (V), molybdenum (Mo), copper (Cu), thorium (Th), and gallium (Ga) (Agnihotri et al., 2003; Tribovillard et al., 2006), had significant cyclic characteristics during glacial-interglacial cycles. To normalize these trace element concentrations, we used the standard approach of dividing trace element concentrations by aluminum (Al) concentrations as an index for the relative enrichment (Bennett and Canfield, 2020). Accordingly, these elements were divided into three categories.

First, the variation range of Mo showed relatively more fluctuation, with value ranges of 0.08–0.61 µg/g. Al (**Figure 4F**). Its distinctly higher values during the Holocene were several times higher than the other peak values in the glacial

stages MIS 10, 8, and 6. Second, U varied from 0.19 to 0.67 µg/g. Al (**Figure 4E**), showing relatively higher values during the glacial stages MIS10, 8, and 6, and a stable tendency since the last 130 kyr. The last category included Cu, Th, Ga, and V, whose ranges were relatively smaller but with obvious cyclic features over glacial-interglacial cycles (**Figures 4A–D**). Most RSEs exhibit a significant enrichment during glacial periods ($p < 0.01$, **Supplementary Table S1**), but Mo and Cu show little enrichment ($p > 0.05$, **Supplementary Table S1**).

3.4 Grain Size Distribution and its End-Member Analysis

Detailed sediment grain size information and original data were derived from Zhang et al. (2020). The detrital distribution of the mean grain size of the sediments varied between 4.49 and 213.16 µm, with a mean value of 17.86 µm to the maximum values of volcanic ash layers (**Supplementary Figure S3A**). Overall, the cyclic variation in mean grain size was finer during glacial periods than during interglacial periods ($p < 0.01$, **Supplementary Table S1**).

The end-member analysis results of grain size showed three end members, with peak modes in the fine (EM1, 5.23 µm), fine to medium (EM2, 19.87 µm), and coarse (EM3, 93.51 µm) particles (**Supplementary Figures S3B–D**). The downcore tendencies of these end-members show different cyclic variations. EM1 variation was consistent with that of the clay content; both were higher during glacial periods and lower during interglacial periods.

4 DISCUSSION

4.1 Variations and Influent Factors of Sedimentary Organic Carbon Input in Glacial-interglacial Cycles
4.1.1 Temporal Variations of Organic Carbon Input
The OC accumulation flux in the study area was comparable to that in other open ocean (Amo and Minagawa, 2003), but much
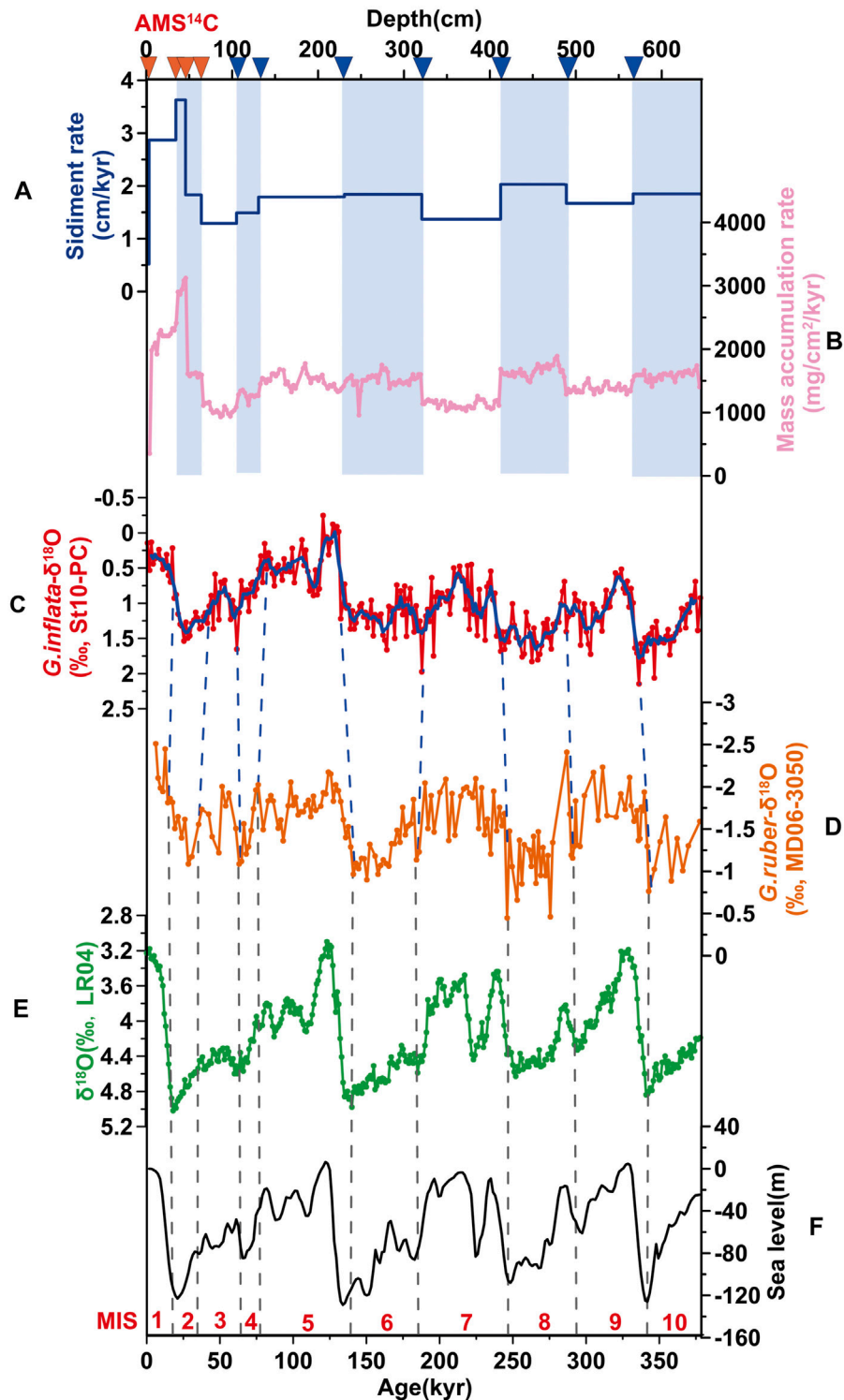
FIGURE 2 | Stratigraphic age model of core St10-PC. **(A)** sedimentary rate of core St10-PC, **(B)** the mass accumulation rate of core St10-PC, **(C)** *G. inflata*-δ^{18}O of core St10-PC with a 5-point running average (blue line) (Zhang et al., 2020), **(D)** *G. ruber*-δ^{18}O of core MD06-3050 (Sun et al., 2011), **(E)** LR04 benthic-δ^{18}O stack (Lisiecki and Raymo, 2005), **(F)** the global sea level variations (Waelbroeck et al., 2002). Orange and blue trangles: age control points of AMS[14]C dating and *G. inflata*-δ^{18}O records of core St10-PC, respectively; blue shadow: glacial periods.
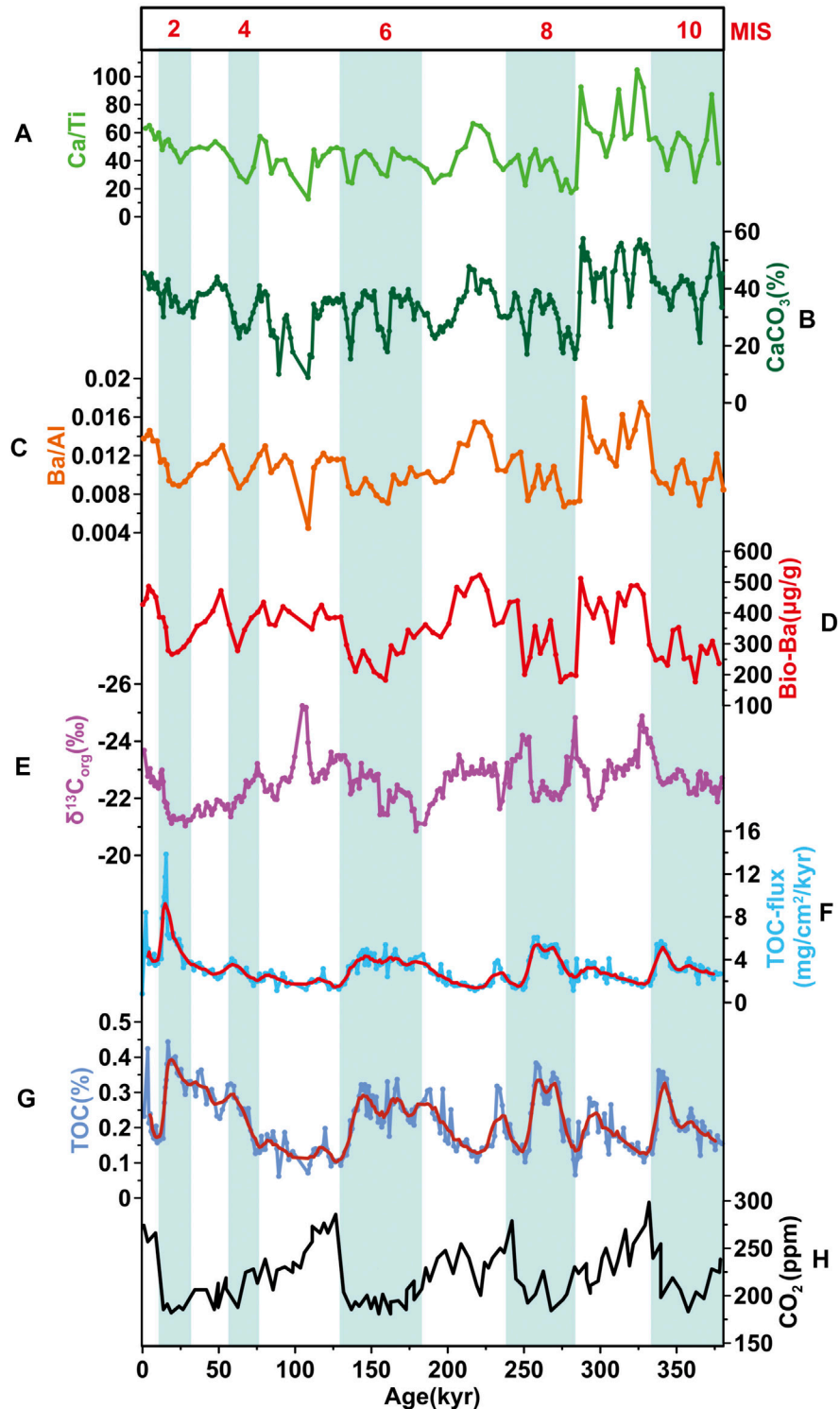
FIGURE 3 | Variation trends of organic carbon flux and its source contribution in core St10-PC. **(A)** Biogenic elements of Ca/Ti ratio, **(B)** biogenic calcium ($CaCO_3$) contents, **(C)** biogenic elements of Ba/Al ratio, **(D)** biogenic barium (Ba_{bio}) contents, **(E)** $\delta^{13}C_{org}$, **(F)** TOC fluxes with a 5-point running average (red line), **(G)** TOC contents with a 5-point running average (red line), **(H)** atmospheric CO_2 concentrations (Lüthi et al., 2008); blue shadow, glacial periods. Original data of OC contents and the $\delta^{13}C_{org}$ were initially from Zhang et al. (2020).
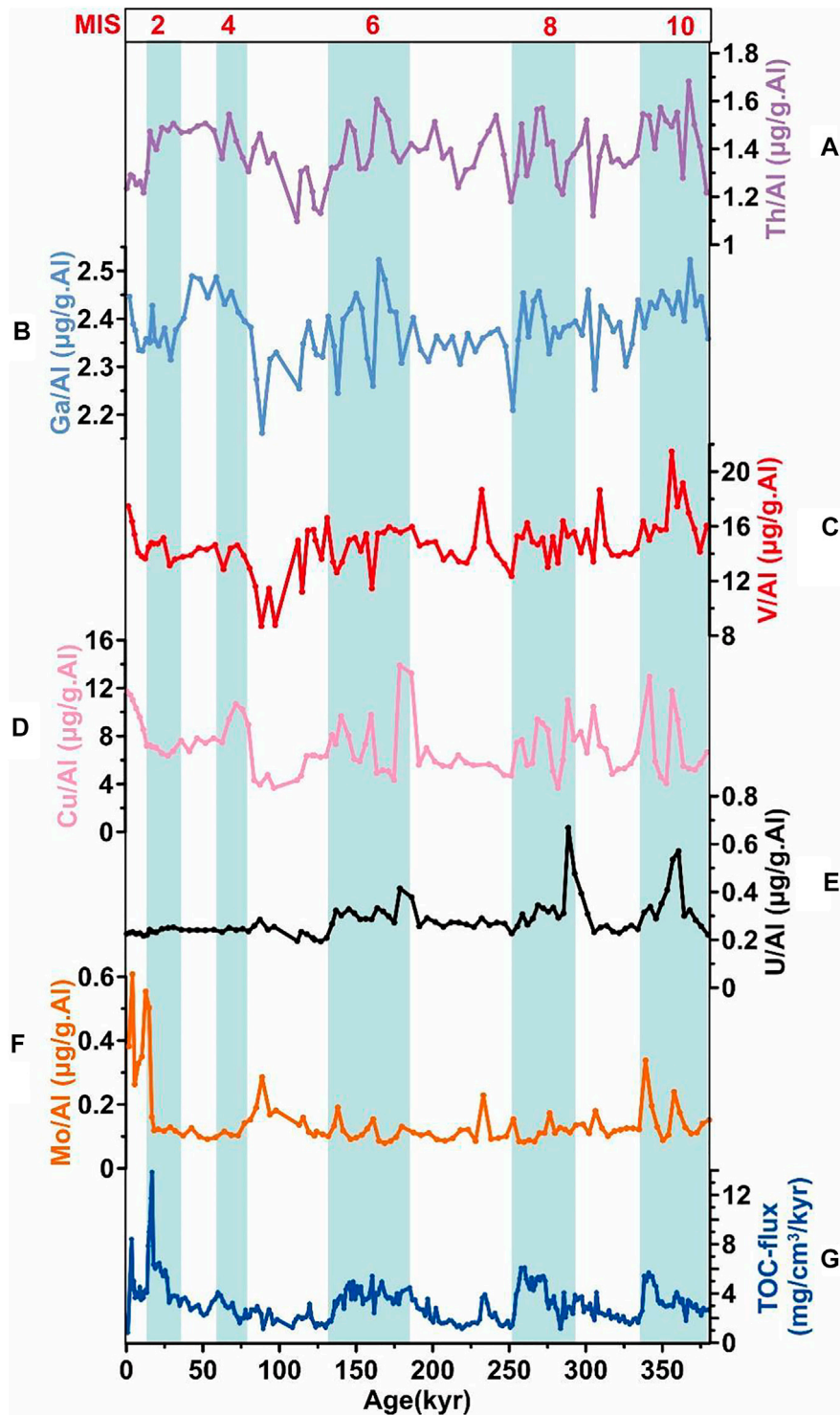
FIGURE 4 | Comparison of RSEs enrichment with TOC in core St10-PC. **(A)** Thorium (Th/Al), **(B)** gallium (Ga/Al), **(C)** vanadium (V/Al), **(D)** copper (Cu/Al), **(E)** uranium (U/Al), **(F)** molybdenum (Mo/Al), **(G)** TOC contents; blue shadow: glacial periods.

lower than that in the continental shelf and basin area (Ikehara et al., 2009; Shao et al., 2016) (**Table.2**). This may be related to the lack of large quantities of terrestrial OC directly delivered by large

rivers and low marine productivity therein. The overall more positive $\delta^{13}C_{org}$ values during glacial periods (**Figure 3E**), indicate that glacial OC input may be mainly derived from

TABLE 2 | Comparison of OC fluxes in cores from the Northwest Pacific Ocean.

Area	Core	Depth (m)	Mean TOC-fluxes (mg/cm^2/kyr)	References
Kyushu Ridge	St10-PC	2670	3.2	This study
Shatsky Ridge	S-2	3107	3.3	Amo and Minagawa, (2003)
Shikoku Basin	PC08	4002	48.4	Ikehara et al. (2009)
Eastern China Sea shelf	ECS12A	1201	310	Shao et al. (2016)

marine-source contributions (Ikehara et al., 2009; Li et al., 2018). Moreover, the alteration of $\delta^{13}C_{org}$ values was affected by diagenesis processes and more depleted with water depth because of the selective degradation of OC (Nakatsuka et al., 1997), which demonstrates the effect of this preservation mechanism on $\delta^{13}C_{org}$ fluctuation. Therefore, more positive $\delta^{13}C_{org}$ values during glacial periods also indicate more marine-sourced OC preservation here in this stage.

However, the distinct peaks of CaCO$_3$ and Ba_{bio} contents (**Figures 3B,D**) observed during interglacials correlated with minima in OC fluxes, indicating paleo-productivity decoupled from OC burial over the past 380 kyr. Under the impact of the formation and enhancement of NPIW in the glacial stages, whose penetration depth hindered the supply of upward macronutrients from deeper water to the euphotic zone (Kohfeld and Chase, 2011; Worne et al., 2019), the observed lower paleo-productivity was similar to other glacial-interglacial cyclic records in the North Pacific (Jaccard et al., 2005; Li et al., 2017; Costa et al., 2018a). Therefore, in the Northwest Pacific, paleo-productivity during glacial periods with the driver of less macronutrient supply from deeper waters (Li et al., 2017) was contrary to that in high nitrate and low chlorophyll (HNLC) areas such as the subantarctic zone, where Fe derived from dust input was the main driver (Martinez-Garcia et al., 2014; Thöle et al., 2019).

4.1.2 Effects of Dust and Kuroshio Current Variation on Organic Carbon Input
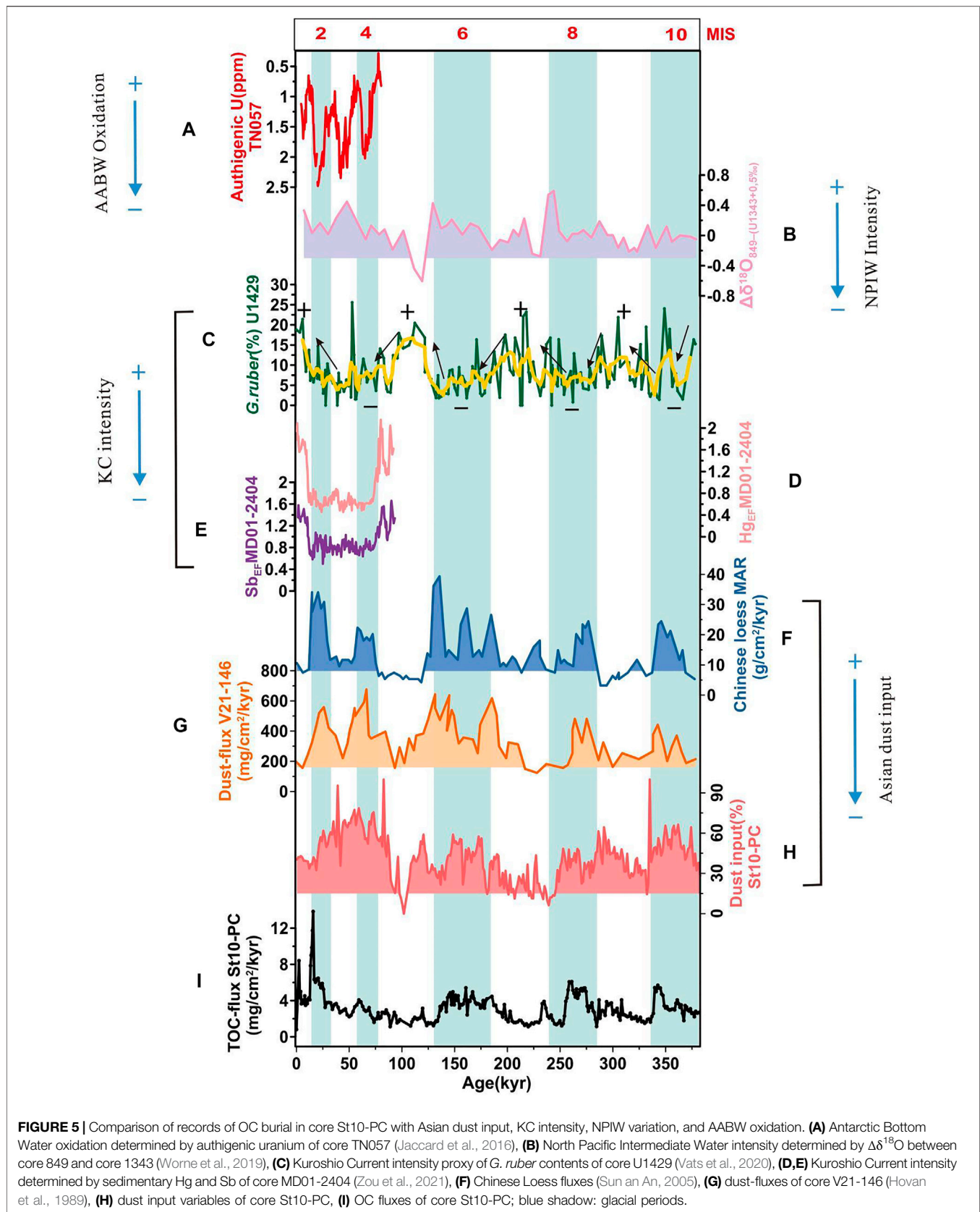
The end-member of sediment grain size was considered as a substitute index for aeolian dust input (Sun et al., 2002). Notably, compared to the dust end-member analysis of core U1438A (Zhou et al., 2016) and core MD06-3050 (Yu et al., 2012) in the Northwest Pacific, we determined that EM1, EM2, and EM3 of core St10-PC may mainly indicate dust input through the westerly and East Asian winter monsoon (EAWM), and the sediment from volcanic ash, respectively (**Supplementary Figure S3B–D**). Moreover, based on the differences in the sources and transfer modes between the westerly and EAWM (Wan et al., 2012; Xu et al., 2015), we assumed that westerly, which carried the dust from a vast area of Asian inland with a longer transport distance than the EAWM, had greater significance in the compositions of these core sediments. Thus, EM1 could be ascribed to the westerly end-member to indicate the overall input of the dust effect around this study area (**Figure 5H**), showing enhanced input during glacial periods ($p < 0.01$, **Supplementary Table S1**) and cohering with other dust fluxes in the North Pacific (e.g., core V21-146, **Figure 5G**, Hovan et al., 1989) and Chinese Loess MAR (**Figure 5F**, Sun and An, 2005).

Based on the intensity of Asian dust input (indicated by EM1 as noted above, **Figure 5H**) over the last 380 kyr, we found that dust input was enhanced in the glacial stages when paleo-productivity decreased (**Figures 3B,D**), which may indicate the limited positive effect of dust input on marine productivity here (Li et al., 2017; Chen et al., 2020). However, higher OC burial in the glacial periods was coherent with dust input (**Figures 5H,I**), which could be attributed to the large area exposure of the East Asian continental shelf during glacial sea-level lowstand, which is more susceptible to erosion and weathering (Wan et al., 2017). Generally, it was easier to deliver more terrestrial materials into this area, resulting in more OC particle input and faster vertical transport to the deep sea during this stage (Cartapanis et al., 2016). This helps to explain the higher OC flux during glacial periods despite the lower marine productivity.

The Kuroshio Current (KC) is a strong western boundary current along the North Pacific and is regarded as an important bridge for transporting heat and material from low to middle and even high latitudes (Ujiié et al., 2003). The modeling simulations indicated that KC intensity was reduced by about 43% as sea level declined during the last glacial maximum, compared to the present day (Kao et al., 2006). The proxies of planktonic foraminifera (*G. ruber*) contents (**Figure 5C**) and surface temperature in core U1429 over the past 400 kyr (Vats et al., 2020) and the proxy for the combination of Hg-Sb enrichment in core MD01-2404 over the past 92 kyr (**Figures 5D,E**, Zou et al., 2021), all reconstructed KC intensity evolution on the orbital scale indirectly, reflecting the significantly decreased KC ($p < 0.05$, **Supplementary Table S1**) when sea temperature decreased and sea level declined during the glacial periods. The "water barrier", an important feature of KC (Zheng et al., 2016), was enhanced during interglacials and obstructed Asian continental sediment transport from the shelf into the deeper ocean (Zhao, 2017). Therefore, the higher OC flux observed in this study was a response to the decreased KC during the glacials, because of more OC transported from the Asian continent under the decreased "water barrier" effect, and better OC preservation under oxygen-poor conditions (detailed in section 4.2).

4.2 Glacial-interglacial Organic Carbon Preservation and Implications for Hydrological Constraint

The decoupling between marine productivity and OC burial, as noted above, could indicate other important constraints on OC burial over glacial-interglacial cycles. It has been suggested that marine biological productivity may contribute less than half of the observed glacial-interglacial variations in OC burial, while the

FIGURE 5 | Comparison of records of OC burial in core St10-PC with Asian dust input, KC intensity, NPIW variation, and AABW oxidation. **(A)** Antarctic Bottom Water oxidation determined by authigenic uranium of core TN057 (Jaccard et al., 2016), **(B)** North Pacific Intermediate Water intensity determined by $\Delta\delta^{18}O$ between core 849 and core 1343 (Worne et al., 2019), **(C)** Kuroshio Current intensity proxy of *G. ruber* contents of core U1429 (Vats et al., 2020), **(D,E)** Kuroshio Current intensity determined by sedimentary Hg and Sb of core MD01-2404 (Zou et al., 2021), **(F)** Chinese Loess fluxes (Sun an An, 2005), **(G)** dust-fluxes of core V21-146 (Hovan et al., 1989), **(H)** dust input variables of core St10-PC, **(I)** OC fluxes of core St10-PC; blue shadow: glacial periods.

physical vertical processes with hydrological constraints may be more responsible for oceanic OC burial (Kohfeld et al., 2005). Hydrological redox conditions control not only microbial growth and activities (Belanger et al., 2020), but also microbial oxidation to OC (Anderson et al., 2019). The first-order impact of microbial oxidization of OC burial depends on the concentration and extent of dissolved oxygen with water depth (Hartnett et al., 1998; Galbraith and Skinner, 2020). Ocean circulation in the Northwest Pacific is complex (**Figure 1B**), with several current systems with different properties at different water depths, including the KC in the upper ocean (Gallagher et al., 2015), the NPIW in the middle (Rippert et al., 2017) and the AABW in deeper water (Kender et al., 2018), which provide different constraints for the dissolved oxygen in the water column over the glacial-interglacial cycles. Therefore, the impact of paleo-redox conditions varying from the upper ocean to the sediment-water interface on OC burial was examined between glacial and interglacial stages.

KC intensity has been shown to have an important impact on OC burial efficiency in the middle Okinawa Trough through changing bottom water O_2 concentration (Li et al., 2018; Zou et al., 2021). As discussed above, the KC was enhanced during the warmer interglacial periods (**Figures 5C–E**, Vats et al., 2020; Zou et al., 2021), which provided higher dissolved oxygen in the upper ocean and had a negative effect on OC preservation (Li et al., 2018). On the other hand, the NPIW is mainly restricted to subtropical North Pacific regions between ~20°N and 40°N and mainly circulates within 300–1000 m of water depth, with the property of low dissolved oxygen (Talley, 1993). The Bering Sea, as the additional source of the Glacial NPIW (Horikawa et al., 2010), resulted in the enhancement of the NPIW formation during the glacial periods (**Figure 5B**). The Glacial NPIW penetrated to deeper range with relatively low oxygen and thus reduced the oxidative decomposition of OC by microorganisms (Worne et al., 2019). Finally, in this area, the extent of dissolved oxygen concentrations in the deep North Pacific is mainly determined by the deeper waters from Southern Ocean (Kender et al., 2018), such as Antarctic bottom water (AABW), which is oxygen-rich (Rippert et al., 2017). Therefore, AABW may have affected OC burial and preservation by changing the redox conditions of the deep ocean. It has been shown that less dissolved oxygen-rich water, indicated by higher authigenic uranium values (**Figure 5A**, Jaccard et al., 2016), moving northward in the glacial periods and contributing to better OC preservation in this stage.

In bottom water, the efficiency of OC degradation at the sediment-water interface, with a loss rate of OC as high as 89.8%, is much higher than that of the transportation in the water column (Ordoñez et al., 2015). Therefore, the effect of redox conditions on OC burial at the sediment-water interface cannot be ignored. The variations in these redox sensitive elements (RSEs) have been used extensively as geochemical proxies to infer the accessibility of dissolved oxygen in the overlying water during the deposition (Bennett and Canfield, 2020). To contextualize the redox conditions through RSE enrichment, we compared the data of this study to a variety of modern depositional environments characterized by the

enrichment of V, U, and Mo (**Table 3**, Bennett and Canfield, 2020). From these observational data at all depths in the global ocean, it can be seen that there was a relatively high variability of enrichment with depth in perennial OMZ (oxygen minimum zone) settings (Scholz et al., 2011), suggesting that water depth may strongly influence redox conditions. The RSE enrichments in core St10-PC characterize a notable increasing tendency with relatively reducing conditions during glacial periods, especially the third category of Th, Ga, V, and Cu, which are in line with the higher sedimentary OC burial during those times (**Figure 4**). Most of these RSEs exist stably in seawater in the form of organometallic ligands (Tribovillard et al., 2006). In the process of sediment settling from the surface to the bottom water, organic matter is easily degraded by microorganisms, during which the complex of RSEs and organic matter is decomposed, and the elements are released back into the water (Morford and Emerson, 1999). Therefore, this noted enrichment of RSEs shows that the sediment-bottom water interface was in a relative reducing state during the glacial periods, with a relatively lower oxygen content in the overlying water, which was more conducive to the burial and preservation of organic matter.

4.3 Glacial-interglacial Regime in Organic Carbon Burial in the Northwest Pacific

To better understand the different patterns of OC burial with different drivers between glacial and interglacial periods, we constructed a conceptual schematic of OC burial and preservation in the mid-latitude Northwest Pacific (**Figure 6**). During glacial periods, despite the increase in dust input and terrestrial matter, the strengthening barrier of glacial NPIW inhibited vertical mixing, slowing transport of nutrient-rich deeper water to the surface (Worne et al., 2019), and thus biological productivity was relatively lower (**Figure 6A**). However, dust input and terrestrial fine-grained materials adsorbed with organic matter to protect and accelerate the deposition of organic matter to the seafloor, where there was a relative reducing condition with less dissolved oxygen content to facilitate OC preservation (Carapanis et al., 2016). In contrast, during interglacial periods (**Figure 6B**), induced by enhanced water column vertical overturning (Worne et al., 2019), the upwelling water brought more nutrients and dissolved oxygen to the surface, which was conducive to phytoplankton photosynthesis. However, under the impact of relative oxidation conditions, microorganisms were relatively active and performed respiration to release organic matter back into the water column (Bennett and Canfield, 2020). Therefore, OC burial was significantly lower in the interglacial periods than in the glacial periods.

Compared to the Northwest Pacific, recent observational records in other areas suggest that the glacial-interglacial regime in OC burial and preservation is likely to be regionally heterogeneous (Carapanis et al., 2016; LaRowe et al., 2020). Carapanis et al. (2016) concluded from hundreds of sediment core records from the global oceans that OC burial pulses derived from higher export production from the surface ocean, higher

TABLE 3 | Comparison of RSEs enrichment in core St10-PC with well-known redox conditions.

Location	Depth (m)	Redox conditions	BW O$_2$ (µM)	Trace elements enrichment degree (µg/g.Al)				References
				V	U	Mo	Re	
Kyushu Ridge	2670	Oxic	/	14.65	0.28	0.15	/	This study
Black Sea	380–1176	Euxinic Basin	0	29 ± 6.3	3.3 ± 0.75	17 ± 4.5	5.0 ± 0.85	Lüschen, (2004)
Namibian Margin	83	Within Perennial OMZ	0	140 ± 73	33 ± 20	41 ± 25	16 ± 5.7	Borchers et al. (2005)
Peruvian Margin	697–2025	Beneath Perennial OMZ	12–93	64 ± 31	5.9 ± 2.3	10 ± 3.6	/	Scholz et al. (2011)
Gulf of California	415–800	Within Seasonal OMZ	/	22 ± 2.5	/	2.6 ± 0.85	/	Brumsack, (1989)
Washington Margin	110–1994	Oxic	25–100	17 ± 0.9	0.4 ± 0.1	0.2 ± 0.03	1.1 ± 0.6	Morford and Emerson, (1999)
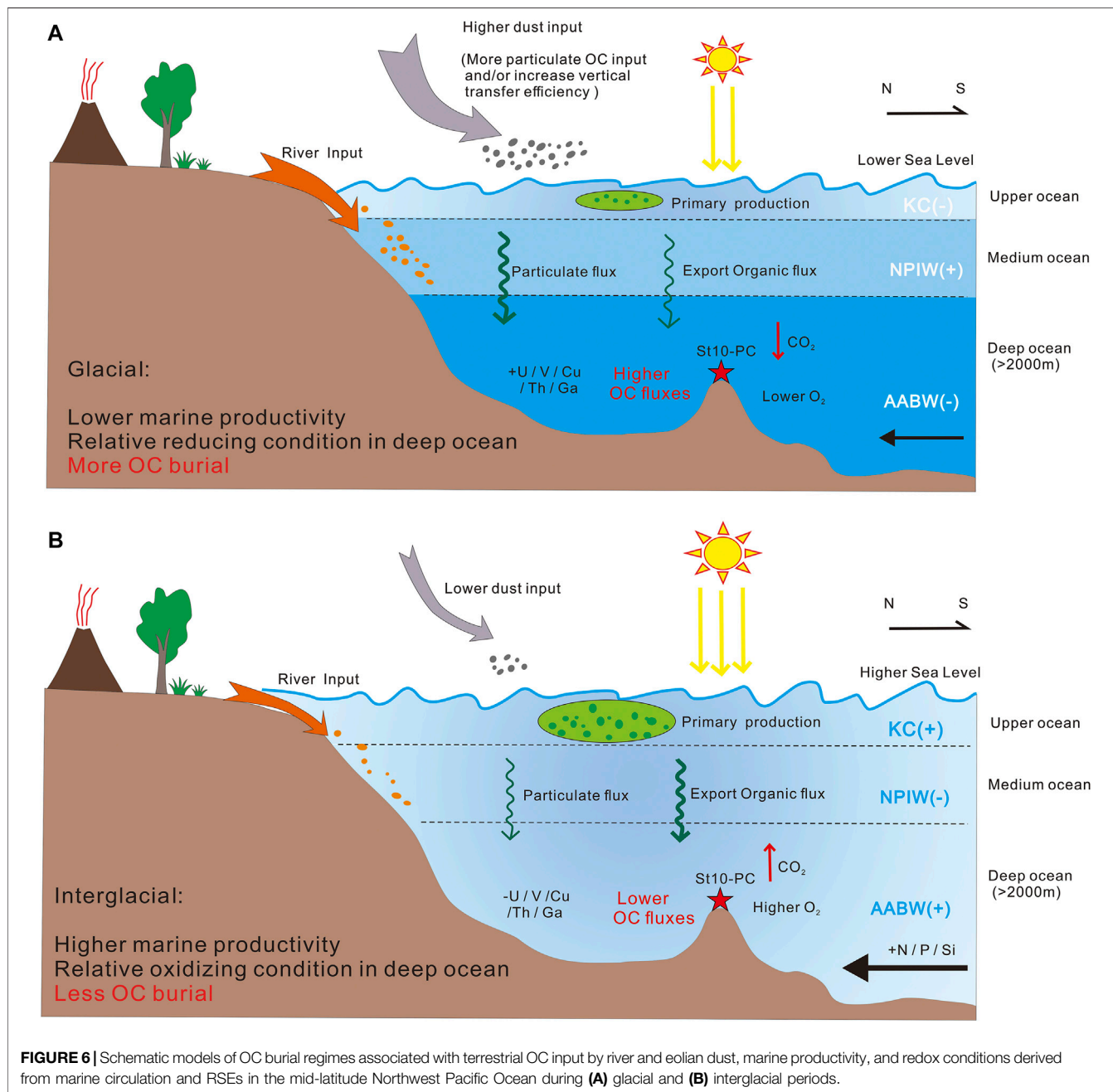
FIGURE 6 | Schematic models of OC burial regimes associated with terrestrial OC input by river and eolian dust, marine productivity, and redox conditions derived from marine circulation and RSEs in the mid-latitude Northwest Pacific Ocean during **(A)** glacial and **(B)** interglacial periods.

transfer efficiency to the deep sea and/or enhanced preservation of organic matter in glacial sediment. Our record of OC burial decoupled from marine productivity and mainly forced by the preservation mechanism and redox conditions, is consistent with observations not only in the Northwest Pacific (Li et al., 2017) but also in the Northeast Pacific (Cristina et al., 2014), where OC burial has been shown to be decoupled from productivity and controlled by the redox conditions and/or other forces. The most controversial and noteworthy issue is the effect of dust input on marine productivity, which may determine how much production in surface waters is exported to the deeper ocean for burial in sediments. Multiple studies in global areas, including the North Pacific (Kienast et al., 2004; Li et al., 2017; Chen et al., 2020) and even the Antarctic Zone (Parekh et al., 2008) and sub-Antarctic Zone (Thöle et al., 2019), have provided evidence for the uncertainties and the limited effects of dust input on primary production, depending on the Fe bioavailability and nutrient availability in different areas (Li et al., 2017; Chen et al., 2020). Our results support that the evolution of marine productivity is not a simple function of OC burial, which reminds us to be cautious in evaluating biological pumps using geological OC records (Li et al., 2018).

In the present study, the water redox conditions could have been a more important driver than marine productivity of OC burial on orbital scale. As mentioned before, the sedimentary redox conditions were oxygen-rich in the Northwest Pacific during interglacial periods relative to the glacial periods, which is similar to the records in the North Pacific (Costa et al., 2018b; Li et al., 2018). Compared to the carbon sink in the surface ocean, carbon preservation in the deeper ocean plays a more prominent role in global climate change in the Northwest Pacific, where extensive and intense circulation in the water column affects carbon degradation (Kienast et al., 2004). Under the influence of such a regime, as mentioned above, our observation of glacial OC burial pulses over the past 380 kyr provides an improved understanding of the global carbon cycle on glacial-interglacial timescales. Its variations throughout Earth's history were highly sensitive to atmospheric CO_2 concentrations (**Figures 3G,H**), implying a notable response of deep-sea OC burial to paleoclimate evolution (Carapanis et al., 2016).

5 CONCLUSION

A comprehensive study of bulk OC fluxes and geochemical features in sediment core St10-PC from the Northwest Pacific was conducted to explore the glacial-interglacial OC burial regime and its environmental implications. Over the past 380 kyr, the notable cyclic variation records show a higher OC burial in the glacial periods, with relatively higher OC input influenced by the dust input and KC, as contrary to the lower biogenic element contents. This is a remarkable phenomenon of decoupling between biogenic production and OC fluxes, suggesting a limited control of the marine productivity on the OC burial in this study area. The enrichment of RSEs at the

sediment-water interface indicated a relatively reducing conditions in glacial periods with higher OC burial flux, which was also closely regulated by the intensity of NPIW and evolution of AABW. Overall, in comparison with interglacial periods, the enhanced OC burial observed in glacial periods emphasize the more important effect of better preservation under reducing conditions. This work further demonstrates pronounced carbon cycle sensitivity to the global climate in the Northwest Pacific on the orbital scale.

DATA AVAILABILITY STATEMENT

The original contributions presented in the study are included in the article/**Supplementary Material**, further inquiries can be directed to the corresponding authors.

AUTHOR CONTRIBUTIONS

YZ, LH, and XS designed the study, synthesized and analyzed the data, and wrote the manuscript with contributions from all authors. YW helped to reconstruct the age model of St10-PC. ZD, ZY, XG, and YL helped to understand the research background related to the sedimentology and paleo-oceanic environment. MI helped to collect the core. All authors contributed to the manuscript and approved its submission.

FUNDING

ACKNOWLEDGMENTS

SUPPLEMENTARY MATERIAL

The Supplementary Material for this article can be found online at: https://www.frontiersin.org/articles/10.3389/feart.2022.886120/full#supplementary-material

REFERENCES

Agnihotri, R., Sarin, M. M., Somayajulu, B. L. K., Jullb, A. J. T., and Burr, G. S. (2003). Late-Quaternary Biogenic Productivity and Organic Carbon Deposition in the Eastern Arabian Sea. *Palaeogeogr. Palaeoclimatol. Palaeoecol.* 197, 43–60. doi:10.1016/S0031-0182(03)00385-7

Amo, M., and Minagawa, M. (2003). Sedimentary Record of Marine and Terrigenous Organic Matter Delivery to the Shatsky Rise, Western North Pacific, over the Last 130 Kyr. *Org. Geochem.* 34, 1299–1312. doi:10.1016/s0146-6380(03)00113-x

Anderson, R., Fleisher, M., and Lao, Y. (2006). Glacial-interglacial Variability in the Delivery of Dust to the Central Equatorial Pacific Ocean. *Earth Planet. Sci. Lett.* 242, 406–414. doi:10.1016/j.epsl.2005.11.061

Anderson, R. F., Sachs, J. P., Fleisher, M. Q., Allen, K. A., Yu, J., Koutavas, A., et al. (2019). Deep-Sea Oxygen Depletion and Ocean Carbon Sequestration during the Last Ice Age. *Glob. Biogeochem. Cycles* 33, 301–317. doi:10.1029/2018GB006049

Belanger, C., Sharon, L., Du, J., Payne, C. R., Mix, A. C., et al. (2020). North Pacific Deep-Sea Ecosystem Responses Reflect Post-glacial Switch to Pulsed Export Productivity, Deoxygenation, and Destratification. *Deep-Sea Res. Part I* 164, 103341. doi:10.1016/j.dsr.2020.103341

Bennett, W. W., and Canfield, D. E. (2020). Redox-sensitive Trace Metals as Paleoredox Proxies: A Review and Analysis of Data from Modern Sediments. *Earth-Science Rev.* 204, 103175. doi:10.1016/j.earscirev.2020.103175

Borchers, S. L., Schnetger, B., Böning, P., and Brumsack, H.-J. (2005). Geochemical Signatures of the Namibian Diatom Belt: Perennial Upwelling and Intermittent Anoxia. *Geochem. Geophys. Geosyst.* 6. doi:10.1029/2004GC000886

Brumsack, H.-J. (1989). Geochemistry of Recent TOC-Rich Sediments from the Gulf of California and the Black Sea. *Geol. Rundsch.* 78, 851–882. doi:10.1007/bf01829327

Cartapanis, O., Bianchi, D., Jaccard, S. L., and Galbraith, E. D. (2016). Global Pulses of Organic Carbon Burial in Deep-Sea Sediments during Glacial Maxima. *Nat. Commun.* 7, 10796–10797. doi:10.1038/ncomms10796

Chen, T., Liu, Q., Roberts, A., Shi, X., and Zhang, Q. (2020). A Test of the Relative Importance of Iron Fertilization from Aeolian Dust and Volcanic Ash in the Stratified High-Nitrate Low-Chlorophyll Subarctic Pacific Ocean. *Quat. Sci. Rev.* 248, 106577. doi:10.1016/j.quascirev.2020.106577

Cheng, X., Huang, B., Jian, Z., Zhao, Q., Tian, J., Li, J., et al. (2005). Foraminiferal Isotopic Evidence for Monsoonal 377 Activity in the South China Sea: a Present-LGM Comparison. *Mar. Micropaleontol.* 54 (1), 125–139. doi:10.1016/j.marmicro.2004.09.007

Costa, K. M., Anderson, R. F., McManus, J. F., Winckler, G., Middleton, J. L., and Langmuir, C. H. (2018b). Trace element (Mn, Zn, Ni, V) and authigenic uranium (aU) geochemistry reveal sedimentary redox history on the Juan de Fuca Ridge, North Pacific Ocean. *Geochimica Cosmochimica Acta* 236, 79–98. doi:10.1016/j.gca.2018.02.016

Costa, K. M., McManus, J. F., and Anderson, R. F. (2018a). Paleoproductivity and Stratification across the Subarctic Pacific over Glacial-Interglacial Cycles. *Paleoceanogr. Paleoclimatology* 33, 914–933. doi:10.1029/2018pa003363

Cristina, L., Kucera, M., and Mix, A. C. (2014). Climate Change Decouples Oceanic Primary and Export Productivity and Organic Carbon Burial. *Proc. Natl. Acad. Sci. U.S.A.* 112 (2), 332–335. doi:10.1073/pnas.1410480111

Dietze, E., Hartmann, K., Bernhard, D., IJmker, J., Lehmkuhl, F., Opitz, S., et al. (2012). An End-Member Algorithm for Deciphering Modern Detrital Processes from Lake Sediments of Lake Donggi Cona, NE Tibetan Plateau, China. *Sediment. Geol.* 243-244, 169–180. doi:10.1016/j.sedgeo.2011.09.014

Galbraith, E. D., and Skinner, L. C. (2020). The Biological Pump during the Last Glacial Maximum. *Ann. Rev. Mar. Sci.* 12, 559–586. doi:10.1146/annurev-marine-010419-010906

Gallagher, S. J., Kitamura, A., Iryu, Y., Itaki, T., Koizumi, I., and Hoiles, P. W. (2015). The Pliocene to Recent History of the Kuroshio and Tsushima Currents: a Multi-Proxy Approach. *Prog. Earth Planet. Sci.* 2, 17. doi:10.1186/s40645-015-0045-6

Hall, I. R., and McCave, I. N. (1998). Glacial-interglacial Variation in Organic Carbon Burial on the Slope of the N.W. European Continental Margin (48°-50°N). *Prog. Oceanogr.* 42, 37–60. doi:10.1016/s0079-6611(98)00027-5

Hartnett, H. E., Keil, R. G., Hedges, J. I., and Devol, A. H. (1998). Influence of Oxygen Exposure Time on Organic Carbon Preservation in Continental Margin Sediments. *Nature* 391 (6667), 572–575. doi:10.1038/35351

Hedges, J. I., Keil, R. G., and Benner, R. (1997). What Happens to Terrestrial Organic Matter in the Ocean? *Elsevier Sci.* 27 (5/6), 195–212. doi:10.1016/s0146-6380(97)00066-1

Hoogakker, B. A. A., Elderfield, H., Schmiedl, G., McCave, I. N., and Rickaby, R. E. M. (2015). Glacial-interglacial Changes in Bottom-Water Oxygen Content on the Portuguese Margin. *Nat. Geosci.* 8, 40–43. doi:10.1038/ngeo2317

Horikawa, K., Asahara, Y., Yamamoto, K., and Okazaki, Y. (2010). Intermediate Water Formation in the Bering Sea during Glacial Periods: Evidence from Neodymium Isotope Ratios. *Geology* 38, 435–438. doi:10.1130/g30225.1

Hovan, S. A., Rea, D. K., Pisias, N. G., and Shackleton, N. J. (1989). A Direct Link between the China Loess and Marine δ18O Records: Aeolian Flux to the North Pacific. *Nature* 340 (6231), 296–298. doi:10.1038/340296a0

Hu, L., Shi, X., Yu, Z., Lin, T., Wang, H., Ma, D., et al. (2012). Distribution of Sedimentary Organic Matter in Estuarine-Inner Shelf Regions of the East China Sea: Implications for Hydrodynamic Forces and Anthropogenic Impact. *Mar. Chem.* 142-144, 29–40. doi:10.1016/j.marchem.2012.08.004

Ikehara, M., Akita, D., and Matsuda, A. (2009). Enhanced Marine Productivity in the Kuroshio Region off Shikoku during the Last Glacial Period Inferred from the Accumulation and Carbon Isotopes of Sedimentary Organic Matter. *J. Quat. Sci.* 24, 848–855. doi:10.1002/jqs.1361

Jaccard, S. L., Galbraith, E. D., Martínez-García, A., and Anderson, R. F. (2016). Covariation of Deep Southern Ocean Oxygenation and Atmospheric CO2 through the Last Ice Age. *Nature* 530, 207–210. doi:10.1038/nature16514

Jaccard, S. L., Haug, G. H., Sigman, D. M., Pedersen, T. F., Thierstein, H. R., and Röhl, U. (2005). Glacial/Interglacial Changes in Subarctic North Pacific Stratification. *Science* 308 (5724), 1003–1006. doi:10.1126/science.1108696

Kao, S. J., Wu, C. R., Hsin, Y. C., and Dai, M. (2006). Effects of Sea Level Change on the Upstream Kuroshio Current through the Okinawa Trough. *Geophys. Res. Lett.* 33, 627–642. doi:10.1029/2006gl026822

Keil, R. G., Tsamakis, E., Wolf, N., Hedges, J. I., and Goni, M. (1997). "Relationships between organic carbon preservation and mineral surface area in Amazon Fan sediments (Sites 932A and 942A)," in *Proceedings of ODP, Scienti*ⁱᶜ *Results* 155. Editors R. D. Flood, D. J. W. Piper, A. Klaus, and L. C. Peterson (College Station, TX: Ocean Drilling Program).

Kender, S., Bogus, K. A., Cobb, T. D., and Thomas, D. J. (2018). Neodymium Evidence for Increased Circumpolar Deep Water Flow to the North Pacific during the Middle Miocene Climate Transition. *Paleoceanogr. Paleoclimatology* 33, 672–682. doi:10.1029/2017pa003309

Kienast, S. S., Hendy, I. L., Crusius, J., Pedersen, T. F., and Calvert, S. E. (2004). Export Production in the Subarctic North Pacific over the Last 800 Kyrs: No Evidence for Iron Fertilization? *J. Oceanogr.* 60 (1), 189–203. doi:10.1023/b:joce.0000038326.73943.aa

Kohfeld, K. E., and Chase, Z. (2011). Controls on Deglacial Changes in Biogenic Fluxes in the North Pacific Ocean. *Quat. Sci. Rev.* 30, 3350–3363. doi:10.1016/j.quascirev.2011.08.007

Kohfeld, K. E., Que´re´, C. L., Harrison, S. P., and Anderson, R. F. (2005). Role of Marine Biology in Glacial-Interglacial CO 2 Cycles. *Science* 308 (5718), 74–78. doi:10.1126/science.1105375

LaRowe, D. E., Arndt, S., Bradley, J. A., Estes, E. R., Hoarfrost, A., Lang, S. Q., et al. (2020). The Fate of Organic Carbon in Marine Sediments - New Insights from Recent Data and Analysis. *Earth-Science Rev.* 204, 103146. doi:10.1016/j.earscirev.2020.103146

Li, D.-W., Chang, Y.-P., Li, Q., Zheng, L., Ding, X., and Kao, S.-J. (2018). Effect of Sea-Level on Organic Carbon Preservation in the Okinawa Trough over the Last 91 Kyr. *Mar. Geol.* 399, 148–157. doi:10.1016/j.margeo.2018.02.013

Li, D., Zheng, L.-W., Jaccard, S. L., Fang, T.-H., Paytan, A., Zheng, X., et al. (2017). Millennial-scale Ocean Dynamics Controlled Export Productivity in the Subtropical North Pacific. *Geology* 45, 651–654. doi:10.1130/g38981.1

Lisiecki, L. E., and Raymo, M. E. (2005). A Pliocene-Pleistocene Stack of 57 Globally Distributed Benthic δ¹⁸O Records. *Paleoceanography* 20, PA1003. doi:10.1029/2004pa001071

Lüschen, H. (2004). *Vergleichende anorganisch-geochemische Untersuchungen an phanerozoischen Corg -reichen Sedimenten: Ein Beitrag zur Charakterisierung ihrer Fazies.* Lower Saxony: University of Oldenburg.

Lüthi, D., Martine Le, F., Bernhard, B., Thomas, B, Jean-Marc, B., Urs, S., et al. (2008). High-resolution Carbon Dioxide Concentration Record 650,000-800,000 Year before Present. *Nature* 453, 379–382. doi:10.1038/nature06949

Maher, B. A., Prospero, J. M., Mackie, D., Gaiero, D., Hesse, P. P., and Balkanski, Y. (2010). Global Connections between Aeolian Dust, Climate and Ocean Biogeochemistry at the Present Day and at the Last Glacial Maximum. *Earth-Science Rev.* 99, 61–97. doi:10.1016/j.earscirev.2009.12.001

Martínez-García, A., Sigman, D. M., Ren, H., Anderson, R. F., Straub, M., Hodell, D. A., et al. (2014). Iron Fertilization of the Subantarctic Ocean during the Last Ice Age. *Science* 343, 1347–1350. doi:10.1126/science.1246848

Milliman, J. D., and Farnsworth, K. L. (2011). *River Discharge to the Coastal Ocean: A Global Synthesis*. Cambridge: Cambridge University Press, 13–69.

Morford, J. L., and Emerson, S. (1999). The Geochemistry of Redox Sensitive Trace Metals in Sediments. *Geochimica Cosmochimica Acta* 63, 1735–1750. doi:10.1016/s0016-7037(99)00126-x

Nakatsuka, T., Handa, N., Harada, N., Sugimoto, T., and Imaizumi, S. (1997). Origin and Decomposition of Sinking Particulate Organic Matter in the Deep Water Column Inferred from the Vertical Distributions of its δ15N, δ13 and δ14. *Deep Sea Res. Part I Oceanogr. Res. Pap.* 44 (12), 1957–1979. doi:10.1016/s0967-0637(97)00051-4

Opsahl, S., and Benner, R. (1997). Distribution and Cycling of Terrigenous Dissolved Organic Matter in the Ocean. *Nature* 386, 480–482. doi:10.1038/386480a0

Ordoñez, C., de la Fuente, A., and Díaz-Palma, P. (2015). Modeling the Influence of Benthic Primary Production on Oxygen Transport through the Water-Sediment Interface. *Ecol. Model.* 311, 1–10. doi:10.1016/j.ecolmodel.2015.05.007

Parekh, P., Joos, F., and Müller, S. A. (2008). A Modeling Assessment of the Interplay between Aeolian Iron Fluxes and Iron-Binding Ligands in Controlling Carbon Dioxide Fluctuations during Antarctic Warm Events. *Paleoceanography* 23, PA4202. doi:10.1029/2007pa001531

Petit, J. R., Jouzel, J., Raynaud, D., Barkov, N. I., Barnola, J.-M., Basile, I., et al. (1999). Climate and Atmospheric History of the Past 420,000 Years from the Vostok Ice Core, Antarctica. *Nature* 399, 429–436. doi:10.1038/20859

Rea, D. K. (2007). Eolian Records, Deep-Sea Sediments. *Encycl. Quat. Sci.*, 643–650. doi:10.1016/b0-44-452747-8/00164-2

Reimer, P. J., Bard, E., Bayliss, A., Beck, J. W., Blackwell, P. G., Ramsey, C. B., et al. (2013). IntCal13 and Marine13 Radiocarbon Age Calibration Curves 0-50,000 Years Cal BP. *Radiocarbon* 55 (4), 1869–1887. doi:10.2458/azu_js_rc.55.16947

Rippert, N., Max, L., Mackensen, A., Cacho, I., Povea, P., and Tiedemann, R. (2017). Alternating Influence of Northern versus Southern-Sourced Water Masses on the Equatorial Pacific Subthermocline during the Past 240 Ka. *Paleoceanography* 32, 1256–1274. doi:10.1002/2017pa003133

Sarnthein, M., Winn, K., Duplessy, J.-C., and Fontugne, M. R. (1988). Global Variations of Surface Ocean Productivity in Low and Mid Latitudes: Influence on CO2 reservoirs of the Deep Ocean and Atmosphere during the Last 21,000 Years. *Paleoceanography* 3, 361–399. doi:10.1029/pa003i003p00361

Schoepfer, S. D., Shen, J., Wei, H., Tyson, R. V., Ingall, E., and Algeo, T. J. (2015). Total Organic Carbon, Organic Phosphorus, and Biogenic Barium Fluxes as Proxies for Paleomarine Productivity. *Earth-Science Rev.* 149, 23–52. doi:10.1016/j.earscirev.2014.08.017

Scholz, F., Hensen, C., Noffke, A., Rohde, A., Liebetrau, V., and Wallmann, K. (2011). Early Diagenesis of Redox-Sensitive Trace Metals in the Peru Upwelling Area - Response to ENSO-Related Oxygen Fluctuations in the Water Column. *Geochimica Cosmochimica Acta* 75, 7257–7276. doi:10.1016/j.gca.2011.08.007

Seo, I., Lee, Y. I., Chan, M. Y., and Kim, H. J. (2014). Sr-Nd Isotope Composition and Clay Mineral Assemblages in Eolian Dust from the Central Philippine Sea over the Last 600 Kyr: Implications for the Transport Mechanism of Asian Dust. *J. Geophys. Res. Atmos.* 119, 11492–11504. doi:10.1002/2014jd022025

Shao, H., Yang, S., Cai, F., Li, C., Liang, J., Li, Q., et al. (2016). Sources and Burial of Organic Carbon in the Middle Okinawa Trough during Late Quaternary Paleoenvironmental Change. *Deep Sea Res. Part I Oceanogr. Res. Pap.* 118, 46–56. doi:10.1016/j.dsr.2016.10.005

Sigman, D. M., and Boyle, E. A. (2000). Glacial/interglacial Variations in Atmospheric Carbon Dioxide. *Nature* 407 (6806), 859–869. doi:10.1038/35038000

Sun, D., Bloemendal, J., and Rea, D. K. (2002). Grain-size Distribution Function of Polymodal Sediments in Hydraulic and Aeolian Environments and Numerical Partitioning of the Sedimentary Components. *Sediment. Geol.* 152 (3), 263–277. doi:10.1016/s0037-0738(02)00082-9

Sun, H., Li, T., Sun, R., Yu, X., Chang, F., and Tang, Z. (2011). Calcareous Nannofossil Bioevents and Microtektite Stratigraphy in the Western Philippine Sea during the Quaternary. *Chin. Sci. Bull.* 56 (25), 2732–2738. doi:10.1007/s11434-011-4603-z

Sun, Y., and An, Z. (2005). Late Pliocene-Pleistocene Changes in Mass Accumulation Rates of Eolian Deposits on the Central Chinese Loess Plateau. *J. Geophys. Res. Atmos.* 110, 1–8. doi:10.1029/2005jd006064

Talley, L. D. (1993). Distribution and Formation of North Pacific Intermediate Water. *J. Phys. Oceanogr.* 23, 517–537. doi:10.1175/1520-0485(1993)023<0517:dafonp>2.0.co;2

Thöle, L. M., Amsler, H. E., Simone, M., Alexandra, A., James, G., Jörg, L., et al. (2019). Glacial-interglacial Dust and Export Production Records from the Southern Indian Ocean. *Earth Planet. Sci. Lett.* 525, 115716. doi:10.1016/j.epsl.2019.115716

Tribovillard, N., Algeo, T. J., Lyons, T., and Riboulleau, A. (2006). Trace Metals as Paleoredox and Paleoproductivity Proxies: An Update. *Chem. Geol.* 232 (1-2), 12–32. doi:10.1016/j.chemgeo.2006.02.012

Ujiié, Y., Asahi, H., Sagawa, T., and Bassinot, F. (2016). Evolution of the North Pacific Subtropical Gyre during the Past 190 Kyr through the Interaction of the Kuroshio Current with the Surface and Intermediate Waters. *Paleoceanography* 31, 1498–1513. doi:10.1002/2015PA002914

Ujiié, Y., Ujiié, H., Taira, A., Toshio, N, and Kazumasa, O. (2003). Spatial and Temporal Variability of Surface Water in the Kuroshio Source Region, Pacific Ocean, over the Past 20,000 Years; Evidence from Planktonic Foraminifera. *Mar. Micropaleontol.* 49, 335–364. doi:10.1016/S0377-8398(03)00062-8

Vats, N., Mishra, S., Singh Raj, K., Gupta, A. K., and Pandey, D. K. (2020). Paleoceanographic Changes in the East China Sea during the Last ~400 Kyr Reconstructed Using Planktic Foraminifera. *Glob. Planet. Change* 189 (2020), 103173.

Waelbroeck, C., Labeyrie, L., Michel, E., Duplessy, J. C., McManus, J. F., Lambeck, K., et al. (2002). Sea-level and Deep Water Temperature Changes Derived from Benthic Foraminifera Isotopic Records. *Quat. Sci. Rev.* 21, 295–305. doi:10.1016/s0277-3791(01)00101-9

Wan, S., and Xu, Z. (2017). Research Progress on Eolian Dust Records in the West Pacific. *Oceanol. Limnologia Sinica* 48 (6), 1208–1219. doi:10.11693/hyhz20170900224

Wan, S., Clift, P. D., Zhao, D., Hovius, N., Munhoven, G., France-Lanord, C., et al. (2017). Enhanced Silicate Weathering of Tropical Shelf Sediments Exposed during Glacial Lowstands: A Sink for Atmospheric CO2. *Geochimica Cosmochimica Acta* 200, 123–144. doi:10.1016/j.gca.2016.12.010

Wan, S., Yu, Z., Clift, P. D., Sun, H., Li, A., and Li, T. (2012). History of Asian Eolian Input to the West Philippine Sea over the Last One Million Years. *Palaeogeogr. Palaeoclimatol. Palaeoecol.* 326-328, 152–159. doi:10.1016/j.palaeo.2012.02.015

Worne, S., Kender, S., Swann, G. E. A., Leng, M. J., and Ravelo, A. C. (2019). Coupled Climate and Subarctic Pacific Nutrient Upwelling over the Last 850,000 Years. *Earth Planet. Sci. Lett.* 522, 87–97. doi:10.1016/j.epsl.2019.06.028

Xu, Z., Li, T., Clift, P. D., Lim, D., Wan, S., Chen, H., et al. (2015). Quantitative Estimates of Asian Dust Input to the Western Philippine Sea in the Mid-late Quaternary and its Potential Significance for Paleoenvironment. *Geochem. Geophys. Geosyst.* 16 (9), 3182–3196. doi:10.1002/2015gc005929

Yoneda, M., Uno, H., Shibata, Y., Suzuki, R., Kumamoto, Y., Yoshida, K., et al. (2007). Radiocarbon Marine Reservoir Ages in the Western Pacific Estimated by Pre-bomb Molluscan Shells. *Nucl. Instrum. Methods Phys. Res. Sect. B Beam Interact. Mater. Atoms* 259 (1), 432–437. doi:10.1016/j.nimb.2007.01.184

Yu, Z., Shi-ming, W., and Sun, H. (2012). Grain-size Records of Asian Eolian Input to the West Philippine Sea over the Last One Million Years. *J. Earth Environ.* 3 (2), 792–800. doi:10.7515/JEE201202005

Zhang, Y., Hu, L., Wu, Y., Yao, Z., Dong, Z., Minoru, I., et al. (2020). Source and Burial of Organic Carbon in the Kyushu-Palau Ridge, Western North Pacific over the Last 400 Ka with its Environmental Implications. *Quat. Sci. (in Chin.* 40 (3), 658–672. doi:10.11928/j.issn.1001-7410.2020.03.06

Zhao, D. (2017). *Sedimentary Evolution in Northern Okinawa Trough and Their Environmental Response since the Last 400ka[D]*. Qingdao: Institute of Oceanology, Chinese Academy of Sciences, 82–98.

Zheng, X., Li, A., Kao, S., Gong, X., Frank, M., Kuhn, G., et al. (2016). Synchronicity of Kuroshio Current and Climate System Variability since the Last Glacial Maximum. *Earth Planet. Sci. Lett.* 452, 247–257. doi:10.1016/j.epsl.2016.07.028

Zhou, Y., Jiang, F., Nan, Q., Liu, H., and Li, A. (2016). Grain-size Distribution of Detrital Sediment in the Amami Sankaku Basin since Late Pleistocene and its Provenance and Paleoclimate Implications. *Adv. Earth Sci.* 31 (3), 298–309. doi:10.11867/j.issn.1001-8166.2016.03.0298

Zhou, Y., Fu-qing, J., and Zhao-kai, X. (2015). Grain-size Distribution of Detrital Sediment in the Parece Vela Basin and its Implication of Provenance and Paleoclimate over the Last 2Ma. *Mar. Sci.* 39 (9), 86–93. doi:10.11759/hykx20140314001

Zou, J., Chang, Y.-P., Zhu, A., Chen, M.-T., Kandasamy, S., Yang, H., et al. (2021). Sedimentary Mercury and Antimony Revealed Orbital-Scale Dynamics of the Kuroshio Current. *Quat. Sci. Rev.* 265, 107051. doi:10.1016/j.quascirev.2021.107051

Zou, J., Shi, X., Liu, Y., Liu, J., Selvaraj, K., and Kao, S.-J. (2012). Reconstruction of Environmental Changes Using a Multi-Proxy Approach in the Ulleung Basin (Sea of Japan) over the Last 48 Ka. *J. Quat. Sci.* 27, 891–900. doi:10.1002/jqs.2578